

James Webb Space Telescope (JWST) Detector Degradation Failure Review Board (DD-FRB)

Executive Summary: Root Cause Determination

DD-FRB Members	
Carl Stahle (Chair)	NASA GSFC, Instrument Systems and Technology Division
Bob Hill (Assistant Chair)	Conceptual Analytics/NASA GSFC, Observational Cosmology Laboratory
Sachidananda Babu	NASA GSFC, Detector Systems Branch
Peter Blake	NASA GSFC, Optics Branch
James Beletic	Teledyne Imaging Sensors
Keith Cleveland	NASA GSFC, Institutional Assurance Branch
Christine Jhabvala	NASA GSFC, Detector Systems Branch
Matt Greenhouse	NASA GSFC, Observational Cosmology Laboratory (ISIM Project Scientist)
Randy Kimble	NASA GSFC, Exoplanets and Stellar Astrophysics Laboratory (I&T Project Scientist)
Robert Kopp	Teledyne Imaging Sensors
Don Lee	Teledyne Imaging Sensors
Henning Leidecker	NASA GSFC, Electrical Engineering Division
Bob McMurray	NASA ARC, Instrument Technology Branch
Judy Pipher	University of Rochester (FGS Detector Scientist)
Eric Piquette	Teledyne Imaging Sensors
Jim Pontius	NASA GSFC, Mechanical Systems Analysis & Simulations Branch
Bernard J. Rauscher	NASA GSFC, Observational Cosmology Laboratory (NIRSpec Detector Scientist)
Marcia Rieke	University of Arizona (NIRCam Principal Investigator)
Bill Tennant	Teledyne Imaging Sensors
Liqin Wang	Ball Aerospace/NASA GSFC, Materials Engineering Branch
Majid Zandian	Teledyne Imaging Sensors
DD-FRB Consultants	
Don Hall	University of Hawaii
Alan Hoffman	Acumen Scientific
Stanley Kohn	Aerospace Corporation
Roger Smith	CalTech
DD-FRB Support	
Emmanuel Cofie	SGT/NASA GSFC Mechanical Systems Analysis & Simulations Branch
Chad Engelbracht	University of Arizona
Don Lindler	SIGMA/NASA GSFC, Exoplanets and Stellar Astrophysics Laboratory
Karl Misselt	University of Arizona
Ray Ohl	NASA GSFC, Optics Branch
Dan Polis	NASA GSFC, Materials Engineering Branch
Christopher Willmer	University of Arizona

29 April 2011

1 Context, Statement of the Problem, and Charter

The JWST science instrument payload contains four science instruments and a fine guidance sensor. Three of the science instruments and the fine guidance sensor utilize HgCdTe detectors that are designed to achieve high responsivity to light over the 0.6–5 micron spectrum. One instrument also utilizes HgCdTe detectors that are designed for the 0.6–2.5 micron spectrum. Seven of the 5 micron cut-off detectors and 8 of the 2.5 micron cutoff detectors are required for flight as shown in Table 1.

Flight model integration has begun on all of the instruments listed in Table 1. Teledyne Imaging Sensors produced all of the JWST HgCdTe detectors during the 2007-8 timeframe. The JWST assembly and test sequence requires that the science instrument detectors have an ambient temperature shelf life of several years prior to launch and an operational life of at least 5.5 years after launch.

Instrument	Agency	Quantity: 5 um cut-off	Quantity: 2.5 um cut-off
NIRCam	NASA	2	8
NIRSpec	ESA	2	NA
FGS-TF	CSA	1	NA
FGS-Guider	CSA	2	NA

Instrument team test data obtained over the past year has revealed degradation of pixel operability impacting several of the 5 and 2.5 micron cut-off detectors. There is a strong concern that the degradation will continue with time and many of the flight arrays will be out of specification by the time of launch. The key detector degradation observed was an order of magnitude increase in the dark count rate of individual pixels to levels in the range of 0.1 to 60 electrons per pixel per second ($e^-/\text{pix}/\text{sec}$). Figure 1 shows an example of this increase in dark count rate for one pixel in a flight spare NIRSpec detector (S060). Other performance anomalies were also observed and are listed in Table 2 at the end of this summary.

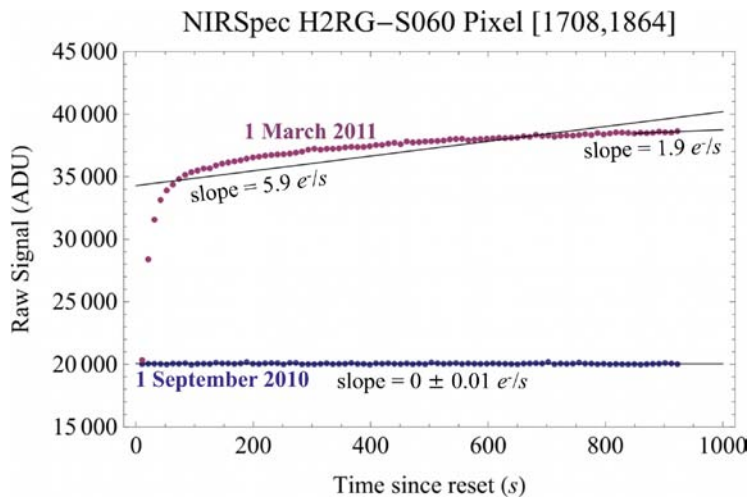


Figure 1. Example of increase in dark count rate for one pixel of a degraded detector. The blue data is for a good pixel and the red data is for the same pixel that has degraded with time.

The JWST Project initiated a Detector Degradation Failure Review Board (DD-FRB) to address the following items:

- (a) Determine the root cause of the detector degradation
- (b) Determine manufacturing and/or post-manufacture handling/process changes to avoid it
- (c) Define tests that are needed to screen-out degradation prone parts and ensure the continued integrity of flight parts
- (d) Define tests to determine whether the existing detectors are qualified for flight

This Executive Summary addresses item (a) only. The DD-FRB will release additional Executive Summaries for items b-d as work progresses. We will write a comprehensive Final Report upon completion of the investigation. Distribution of summaries covering items (b), (c), and the Final Report will be subject to Teledyne proprietary and ITAR data restrictions.

2 Root Cause Determination

The DD-FRB finds that the detector degradation is caused by a **design flaw in the barrier layer** of the pixel interconnect structure. The flawed barrier layer design makes the detectors vulnerable to migration of indium from the indium bump interconnect into the detector structure, degrading its performance.

The most obvious effect is the formation of an indium (In) gold (Au) intermetallic that is highly visible in Scanning Electron Microscopy (SEM) images taken during destructive physical analysis. The electrical data of degraded pixels reveal curved, "RC" shaped dark ramps that are indicative of parasitic capacitance, reactance, and shunting in the HgCdTe side of the interconnect. Typically a few hundred seconds after reset, true leakage currents become dominant. These effects cause pixels to fail to meet operability requirements.

Figure 2a shows a cross-section of the pixel contact structure design. In this sensor design, each HgCdTe pixel is connected via the In bump to a source-follower amplifier in a silicon Read-Out Integrated Circuit (ROIC). The critically important barrier layer is intended to prevent In bump material from reacting with the Au pad and Au contact material such that it can not diffuse into the HgCdTe detector material. Figures 2b and 2c show cross-sectional micrographs obtained with SEM of a non-degraded pixel from a 2.5 micron NIRCcam detector array (C105) and a degraded pixel from a 5 micron NIRCcam detector array (C094). The cross-section of the pixel structure was generated by destructive physical analysis (DPA) using a focused ion beam (FIB) to cut through a line of pixels in the array. Figure 2c shows the formation of an AuIn₂ intermetallic as well as a crack in the left corner of the pixel contact structure propagating into the HgCdTe detector. The

intermetallic expands upon formation and most likely created a pocket of stress in the pixel.

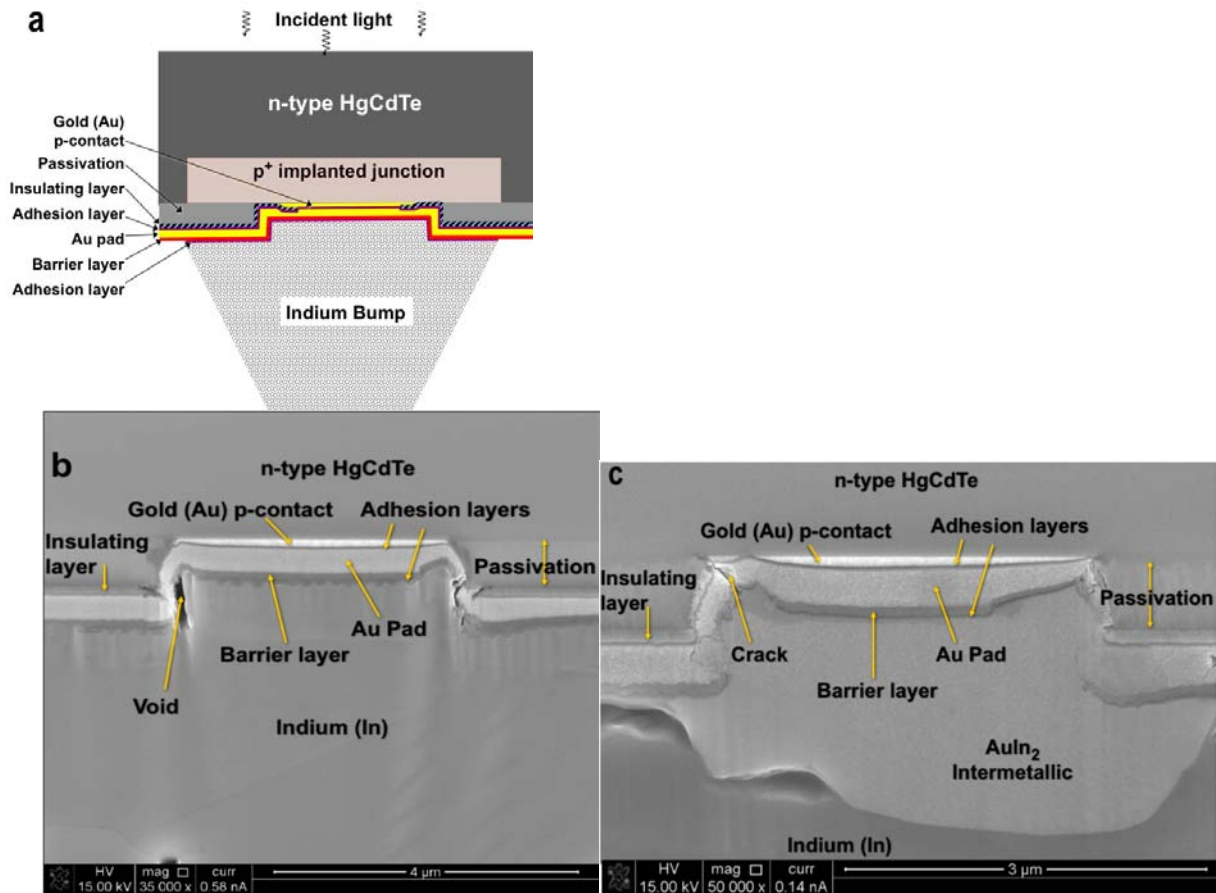


Figure 2. a) Pixel contact structure; b) Scanning Electron Microscope (SEM) image of a non-degraded pixel in NIRCcam detector C105; c) SEM of degraded pixel in NIRCcam detector C094

Figure 3(a) shows a diagram depicting failure of the barrier layer. Poor sidewall coverage of the layers over the step of the passivation layer or porosity of the barrier layer can allow In to inter-diffuse with the Au contact and Au pad metals to create In-Au intermetallics. Figure 3(b) illustrates some potential degradation mechanisms; the intermetallic expansion may cause strain and lattice dislocation damage to the HgCdTe and/or enable In to diffuse into the p⁺ HgCdTe of the implanted junction layer. Apart from production of charge traps in the semiconductor band gap, dislocation damage can also allow In or Au to diffuse more rapidly into the HgCdTe resulting in a dark current performance degradation rate that can be non-linear and difficult to reliably estimate.

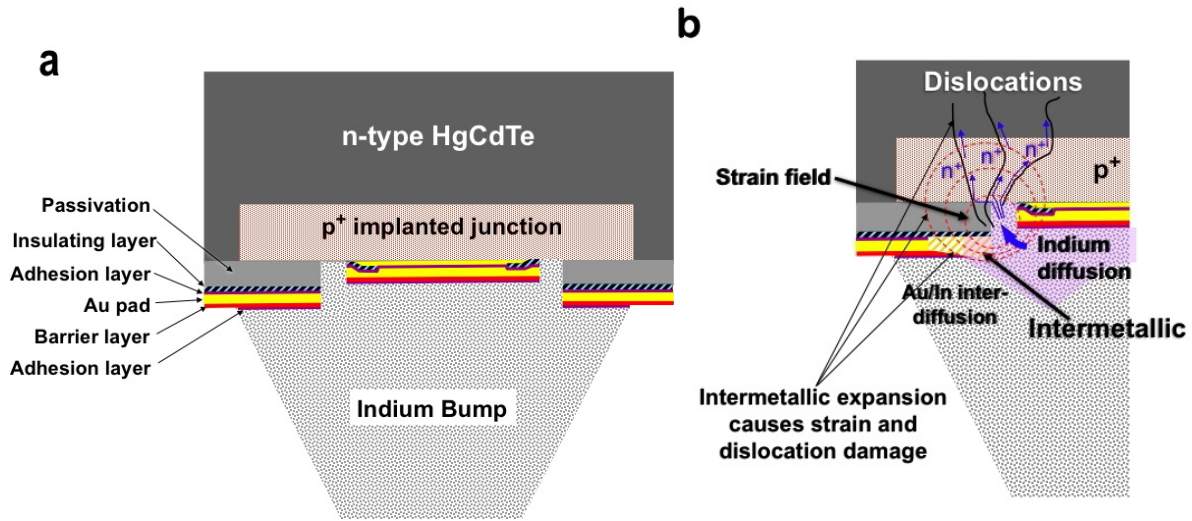


Figure 3. (a) Inadequate barrier layer coverage; (b) Potential degradation mechanisms

Figure 4 shows the flow diagram of the degradation mechanisms.

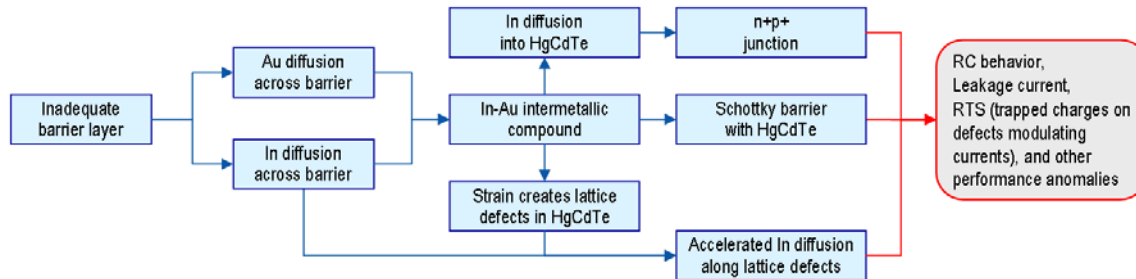


Figure 4. Degradation process in a pixel due to inadequate barrier layer

A degraded detector pixel can be modeled by an electrical circuit, which produces an integration ramp signal with an “RC”-like curvature early in the ramp (see Fig. 1). More extensive damage or indium diffusion will produce additional leakage currents through the photodiode. Although this circuit model approximately captures the essential behavior of degraded pixels (an “RC” at early times and leakage at later times), the actual circuit elements are far from ideal.

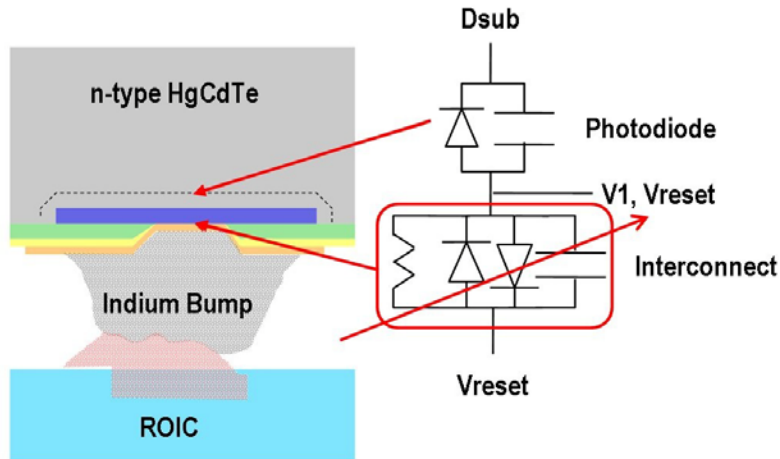


Figure 5. This electrical circuit model of a degraded pixel accounts for the “RC”-like curvature of dark ramps (see Fig. 1). The red-highlighted components form in the HgCdTe immediately above the failed barrier layer. These cause the “RC”-like shape. This simple model does not attempt to explain the degradation in the photodiode that causes enhanced leakage current.

Formation of the In-Au intermetallic was confirmed by Energy Dispersive x-ray Spectroscopy (EDS) to provide a direct measure of the elemental composition. Figure 6a shows a SEM image of a corner of another detector pixel in detector array C094 with a corresponding elemental map for Au, In, and the barrier layer in Figure 6b. For these samples, the cross-section was prepared by cutting through the sample with a wire saw followed by mechanical polishing. The data show the formation of the In-Au intermetallic with a break in the barrier layer at the sidewall of the contact opening.

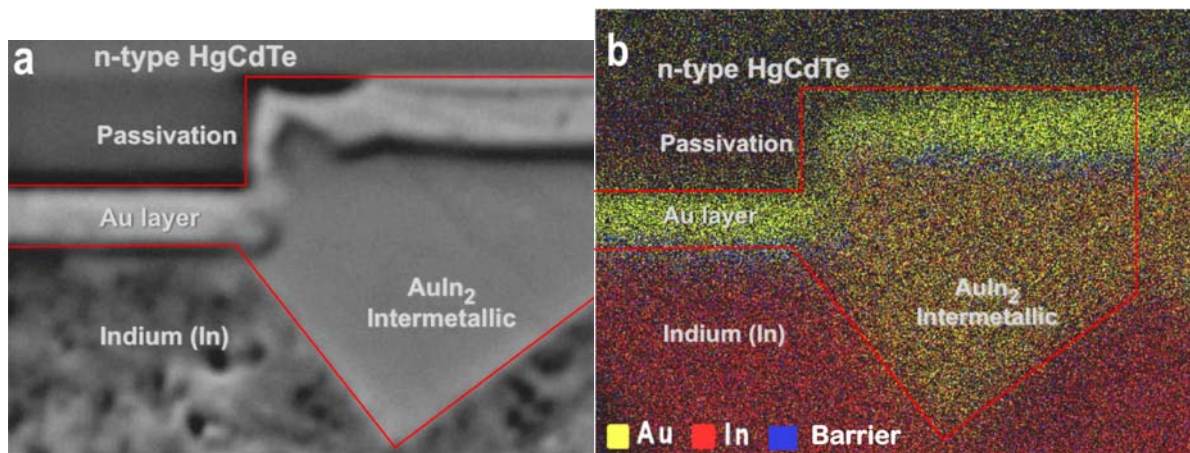


Figure 6. a) SEM of a pixel corner in NIRCcam detector C094; b) X-ray elemental analysis (EDS) of the same area showing that Au and In have interdiffused to form an intermetallic compound ($AuIn_2$) due to failure of the barrier layer

Additional EDS data was taken on another pixel in detector C094 as well as the Process Evaluation Chip (PEC) for C094. Figure 7a shows the SEM and the x-ray analysis area (red box) from the PEC and Figure 7b shows the x-ray spectrum. Quantitative analysis of the weight percentage of the volume measured shows that the In-Au compound is AuIn_2 .

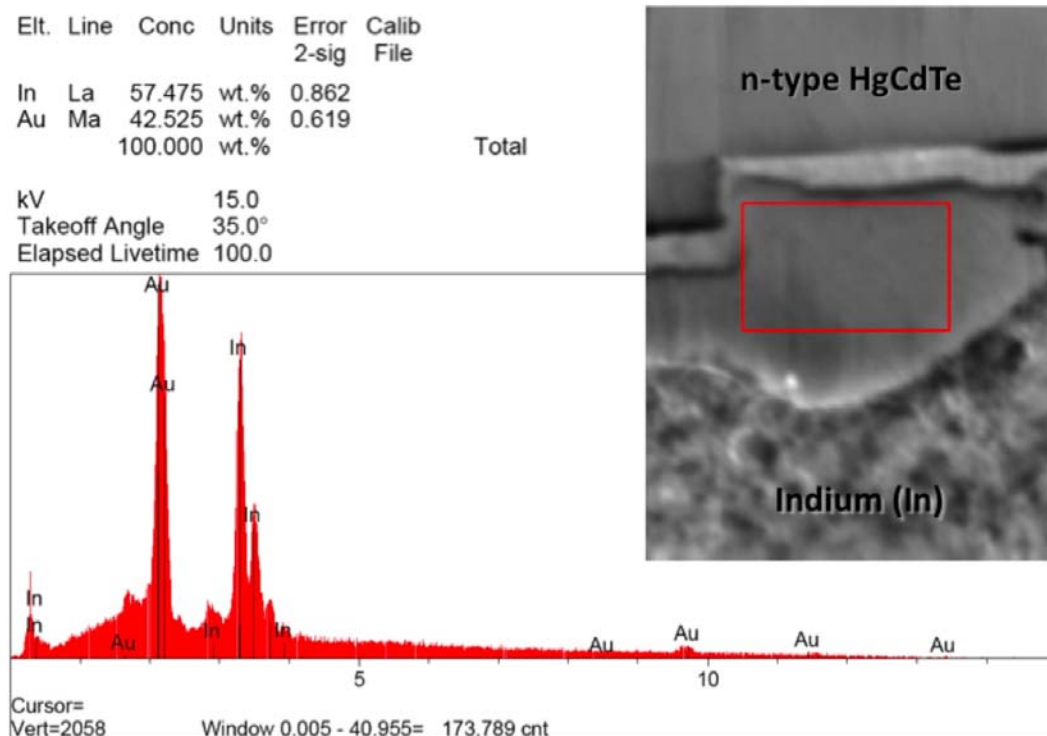


Figure 7. a) X-ray analysis (EDS) of red box area in SEM image demonstrates the formation of an In-Au intermetallic (AuIn_2)

Figure 8 shows a SEM image and a backscatter electron image of a cross-section of a pixel in detector array C094. Combined with EDS analysis on the different regions, the results show that there is interdiffusion of both In and Au past the barrier layer with the formation of AuIn_2 and AuIn intermetallics that expand in volume.

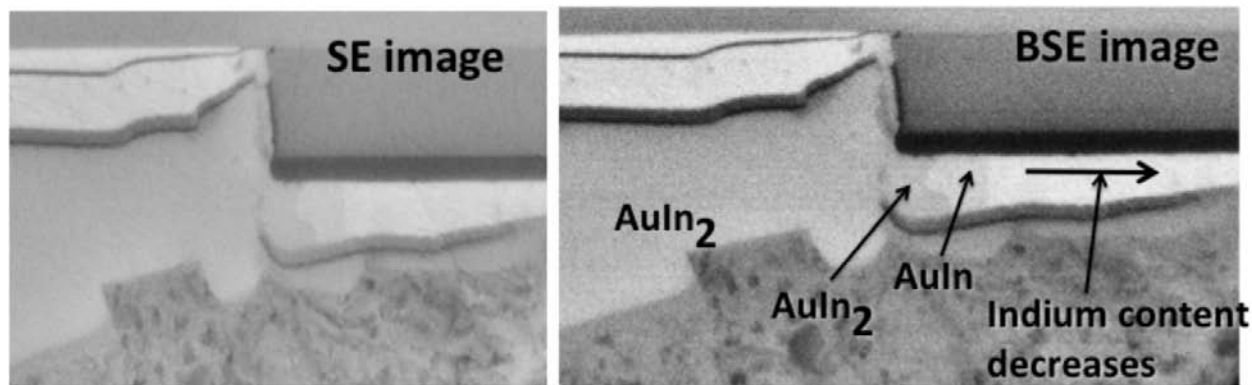


Figure 8: SEM and Backscatter Secondary Electron (BSE) image of detector pixel in C094

3 Key Physical Observations that Support Root Cause

To avoid focusing on a single aspect of the observed degradation, the DD-FRB developed a list of key observations that any root cause analysis would have to explain. This list began at 14 items and has since grown to 25 items, with each new observation adding or reinforcing the list (Table 2). There are some common elements for all explanations:

1) formation for an RC circuit element, most likely an n/p or Schottky barrier that completely intercepts the circuit after the contact; and 2) defects which increase the detector junction leakage current. These common elements are likely caused by damage (dislocations, displaced ions) induced by the intermetallic formation itself due to an inadequate barrier layer. The damage is further increased in its effect by enhanced diffusion of indium, now present at or in the HgCdTe from the proximate In-Au intermetallic. Beyond this, every diode will have its own story, and there are millions of them in a detector array. Further details of the physical mechanisms by which these various observations can arise will be provided in the final report of the DD-FRB.

4 Path Forward

Summary findings for charter items (b-d) above are in progress. At this juncture, the DD-FRB believes that a specific and practical method for fabrication of a fully effective barrier layer is available at Teledyne Imaging Sensors to eliminate the above design flaw in newly manufactured detectors. This design was developed for a higher background application than space astrophysics, and further testing is required to show that it can meet JWST performance requirements. The Board anticipates recommendation of screening and accelerated life tests to verify the long-term effectiveness of this solution. Finally, the Board anticipates recommendation of specific tests to assess the flight worthiness of JWST HgCdTe detectors that do not currently exhibit out-of-spec performance.

Table 2: Key Physical Observations

Table 2: Key Physical Observations	
Warm (degraded) pixel: A pixel with a dark count rate $0.1 < \text{rate} < 60$ e-/sec, where the count rate is measured using a linear 2-parameter fit to the up-the-ramp samples spanning 1000sec.	
Degraded detector: A detector that exhibits a statistically significant increase in the number of warm pixels.	
1	The number of warm pixels increases with time in both the 2.5 μm and 5 μm cutoff detectors that show degradation.
2	In degraded detectors, some warm pixels get better at the same time as a larger number get worse.
3	The rate of degradation of the detectors varies from part to part and is not necessarily linear with time.
4	Although clustered, the new warm pixels do not form a contiguous group.
5	The spatial distribution of the warm pixels appears to be similar for all the NIRCcam 5 μm detectors. In addition, there are similarities in the spatial distribution of warm pixels among the affected NIRSpec detectors, but the distributions are different from those of the NIRCcam parts. However, there is at least one small area near the edge of the detectors with a higher density of warm pixels that is common to both the NIRCcam and NIRSpec parts.
6	No warm pixels have been observed in the reference pixels of any degraded detector, even though new warm pixels are seen in the immediately adjacent regions of some degraded detectors.
7	Areas with an increased density of warm pixels also show a small decrease in flat field response relative to "good" regions.

8	While some new warm pixels may be hot pixel neighbors, most new warm pixels are not related to hot pixels.
9	The regions with high densities of new warm pixels are preferentially found near the edges of the detectors rather than at the centers. These regions are also where the stress-induced curvature of the detectors is at a minimum.
10	A 12hr bake at 50C in a dry nitrogen environment resulted in an increased number of warm pixels, indicating an increased rate of formation while at elevated temperature in one of the degraded NIRCcam 5 μ m detectors (C094).
11	The new warm pixels that appeared after the 12hr-50C bake of C094 have a similar spatial distribution and electrical properties (dark count rates, ramp shapes) as the pixels that had become warm during ambient storage.
12	The character of the degradation of some WFC3 detectors at their operating temperature of 145K is very similar to that of the JWST detectors at their ~40K operating temperature, despite the differences in the long wavelength cut-off (1.7 μ m vs. 5 μ m), processing details, and subsequent storage and handling. It is possible that the same physical processes are at work in both instances, while the details may differ.
13	Eight of the eleven tested 5 μ m detectors show degradation. However, only two out of thirteen 2.5 μ m detectors have degraded. In addition, two FGS 5 μ m detectors show no degradation but have been stored in ambient conditions for ~1 year less than the other JWST detectors.
14	The slope of the dark signal ramps for most (80-85%) new warm pixels shows statistically significant curvature (RC-like behavior).
15	For a large fraction of the new warm pixels in NIRSPEC detector S060 (5 μ m), the dark count rate is approximately independent of temperature at low temperatures (T < 80K). However, at higher temperatures (80-100K), a dependence of the dark count rate on temperature is observed, indicating that a different mechanism is dominant in each of the two temperature regimes.
16	A change in temperature from 37.5K to 41K can result in some apparently good pixels becoming bad for S060.
17	Under the assumption of normal gain, the noise in some, or all, new warm pixels, while higher than for good pixels, is lower than expected from shot noise associated with the measured signal.
18	For S060, the asymptotic value of the dark count rate is consistent with the noise enhancement in degraded pixels. For this detector, the degradation manifests as a) the appearance of an "RC behavior" shortly after reset, and b) real leakage current that dominates the "RC" after a few hundred seconds.
19	The two 2.5 μ m detectors (C038 & C041) that have exhibited an increase in warm pixels show an even larger fraction of warm pixels (relative to the mean) when measured at higher temperatures (90K for C038 and 85K for C041).
20	The region of C038 that exhibits an increased density of warm pixels (at both 39.5K and 90K) also shows a decrease in well depth.
21	Most of the warm pixels in C041 become good when the detector is cooled to 23.4K.
22	Multiple labs have observed the same phenomena in different test sets.
23	The Scanning Electron Microscope (SEM) and Energy Dispersive x-ray Spectroscopy (EDS) analysis of C094 shows that an In-Au intermetallic has formed in all 15 pixels examined to date. These include examples of both degraded and non-degraded pixels. SEM analysis of the Process Evaluation Chip (PEC) associated with this detector also shows the In-Au intermetallic in all pixels examined. The major intermetallic formed is AuIn ₂ . AuIn is also formed next to the AuIn ₂ where there was originally Au.
24	SEM analysis of the PEC associated with the good (i.e. showing no degradation) 2.5 μ m detector C105 shows no indication of In-Au intermetallic formation.
25	SEM analysis of the PEC associated with the 5 μ m detector S042 shows that an In-Au intermetallic has formed, although the intermetallic volume appears to be less than in C094. This detector has shown no degradation as of the most recent testing in Jan. 2010.

